Accepted Manuscript

Combining padlock exponential rolling circle amplification with $CoFe_2O_4$ magnetic nanoparticles for microRNA detection by nanoelectrocatalysis without a substrate

Nan Yu, Zhen Wang, Chaochen Wang, Jing Han, Huaiyu Bu

PII: S0003-2670(17)30179-4

DOI: 10.1016/j.aca.2017.01.069

Reference: ACA 235062

To appear in: *Analytica Chimica Acta*

Received Date: 3 December 2016

Revised Date: 22 January 2017

Accepted Date: 27 January 2017

Please cite this article as: N. Yu, Z. Wang, C. Wang, J. Han, H. Bu, Combining padlock exponential rolling circle amplification with $CoFe_2O_4$ magnetic nanoparticles for microRNA detection by nanoelectrocatalysis without a substrate, *Analytica Chimica Acta* (2017), doi: 10.1016/j.aca.2017.01.069.

Graphical Abstract

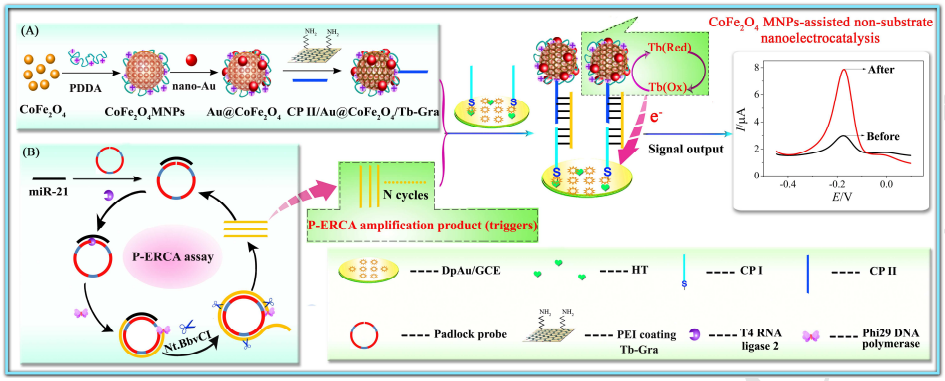

Combining padlock exponential rolling circle amplification with $CoFe_2O_4$ magnetic nanoparticles for microRNA detection by nanoelectrocatalysis without a substrate

Nan Yu [a,1], Zhen Wang [b,1], Chaochen Wang [a], Jing Han [b,*], Huaiyu Bu [a,*]

[a] *Shaanxi Provincial Key Laboratory of Biotechnology, Key Laboratory of Resource Biology and Biotechnology in Western China (Ministry of Education), Northwest University, Xi'an 710069, P. R. China.*

[b] *Key Lab of Synthetic and Natural Functional Molecule Chemistry of Ministry of Education, College of Chemistry and Materials Science, Northwest University, Xi'an, Shaanxi 710127, P. R. China.*

[1] *These authors contributed equally to this work.*

ABSTRACT

In this report, an ultrasensitive electrochemical biosensor for miR-21 detection was designed on the basis of a padlock exponential rolling circle amplification (P-ERCA) assay and $CoFe_2O_4$ magnetic nanoparticles ($CoFe_2O_4$ MNPs) by nanoelectrocatalysis without a substrate for signal amplification. Here, to improve catalytic efficiency, nanocatalyst ($CoFe_2O_4$ MNPs) and redox molecule (Tb) were co-immobilized onto the graphene (Gra) surface and formed Au@$CoFe_2O_4$/Tb-Gra

* Corresponding author.

E-mail address: hanjing@nwu.edu.cn (J. Han), buhy@nwu.edu.cn (H. Bu).

probe. The obtained probe exhibits high-performance Tb catalysis by reducing the interaction distance between $CoFe_2O_4$ MNPs and Tb, and importantly, the detection sensitivity is significantly improved even in the absence of substrate (H_2O_2). Simultaneously, to further improve the sensitivity and specificity of the biosensor, P-ERCA assay was introduced. After multiple polymerization and nicking reactions, plenty of P-ERCA amplification product was produced and circular exponential signal amplification was achieved, giving an extreme sensitivity for miR-21 assay. The as-prepared biosensor shows a wide dynamic range of 1 fM to 2 nM with a low detection limit of 0.3 fM for miR-21 detection and exhibits high specificity and sensitivity.

***Keywords*:** $CoFe_2O_4$ MNPs; Nanoelectrocatalysis; P-ERCA assay; Electrochemical biosensor; MicroRNA.

1. Introduction

MicroRNAs (miRNAs), a series of short, endogenous and noncoding RNAs (about 22 nucleotides), are crucial regulators of gene expression [1,2]. Recent studies have revealed that the expression of miRNAs could provide crucial information for early diseases diagnosis, such as cancers, cardiovascular diseases and neurological disorders, etc. [3-5]. Thus, miRNAs have been regarded as important biomarkers in the study of diseases diagnostic and prognostic processes. Nevertheless, there remain major challenges in the selective and sensitive determination of miRNA because of its small size, low-level expression and highly homologous sequences [3,6]. Routine techniques, including northern blotting [7] and microarray-based hybridization [8,9]

are often encounter limitations such as low specificity, poor reproducibility and sophisticated instrumentations. Therefore, a detection technique capable to measure miRNA in a reliable manner with high specificity and sensitivity is intensely demanded.

Electrochemical biosensors as an important research area of analytical chemistry have received considerable attention as their inherent advantages of high sensitivity, fast response as well as good portability [10-12]. To improve the detection sensitivity, various electrochemical biosensors based on nucleic acid amplification, such as rolling circle amplification (RCA) [13,14], loop-mediated isothermal amplification (LAMP) [15] and strand displacement amplification (SDA) [16] have been successfully fabricated. Among them, RCA is a simple and reliable amplification method, which has become increasingly popular in miRNA detection [17-19]. Tang's group [20] recently developed new padlock exponential rolling circle amplification (P-ERCA) based on RCA for the fluorescent detection of miRNA with higher specificity and sensitivity down to the zmol level. As we know, to date, P-ERCA has rarely been applied in electrochemical assays for miRNA detection.

On the other hand, to further improve the sensitivity of the biosensor, nanomaterials as nanozyme-assisted signal amplification strategies were widely used recently in biomolecular detection [21-23]. For instance, amount of carbon-based materials, cerium oxide and metal oxides have been reported to exhibit artificial enzyme activity [24-26]. Among these nanozymes, magnetic nanoparticles (e.g. Fe_3O_4 MNPs, $CoFe_2O_4$ MNPs) are particularly interesting because they not only exhibit an

intrinsic peroxidase-like activity with H_2O_2 substrate [27-29], but also act as nanoelectrocatalyst (e.g. thionine, methylene blue) for signal amplification even in the absence of H_2O_2 [30]. Importantly, magnetic nanoparticles benefit from the advantages of better magnetic separation, nontoxicity and easy synthesis in comparison with conventional artificial enzymes [31-33].

In this contribution, we present a highly specific and sensitive biosensor by combining P-ERCA assay with $CoFe_2O_4$ MNPs for microRNA detection based on nanoelectrocatalysis without a substrate. As shown in Fig.1, in the presence of miR-21, the padlock probe could specifically hybridize with it through complementary base pairing and further connecting to form a loop head-to-tail with the help of T4 RNA ligase 2. Once miR-21 and the padlock probe form a complex, a long DNA fragment concatenated sequence copy of the padlock probe was obtained with the assistance of Phi29 DNA polymerase. After multiple polymerization and nicking reactions, plenty of new triggers (P-ERCA amplification product) were produced and circular exponential signal amplification was achieved, thus giving an extremely sensitive method for miR-21 assay. The electrochemical biosensing interface was constructed by simple immobilization of capture probe I (CP I) on the electrochemically deposited $HAuCl_4$ modified electrode. Simultaneously, Au@$CoFe_2O_4$/Gra-Tb composites were employed to the immobilization of capture probe II (CP II) forming CP II bioconjugate (CP II/Au@$CoFe_2O_4$/Gra-Tb). With the help of triggers, CP II/Au@$CoFe_2O_4$/Gra-Tb was further introduced onto the CP I modified electrode surface through specific complementary sequences. As a result, the detection signal

was obtained from $CoFe_2O_4$ MNPs to high-performance redox molecule (Tb) catalysis. The $CoFe_2O_4$ MNPs-assisted signal amplification without a substrate, exhibits a remarkable sensitivity for miR-21 detection. Furthermore, the proposed assay provides a versatile method for other miRNAs or DNA detection by slightly changing the corresponding probe sequences.

Fig. 1

2. Experimental section

2.1. Reagents and materials

T4 RNA ligase 2, Phi29 DNA polymerase and Nt.BbvCI were received from New England Biolabs (Ipswich, USA), and dNTP mixture was purchased from Takara (Dalian, China). Gold chloride ($HAuCl_4$), polyethyleneimine (PEI), toluidine blue (Tb), polyethylene glycol (PEG), poly (diallyldimethylammonium chloride) (PDDA, 20 *wt*% in water, MW: 200 000-350 000) and hexanethiol (HT) were supplied by Sigma Chemical Co. (St. Louis, USA). Ethylene glycol and other chemical reagents are analytical reagent (A.R.) grade.

The buffers involved in this work were prepared as below: Probe immobilization buffer (IB, pH 7.4) contained 10 mM Tris-HCl, 1.0 mM ethylenediaminetetraacetic acid (EDTA), 10 mM tris(2-carboxyethyl)phosphine hydrochloride (TCEP) and 0.1 M NaCl. DNA hybridization buffer (HB, pH 7.4) contained 10 mM Tris-HCl, 1.0 mM EDTA and 1.0 M NaCl. HAc-NaAc (0.1 M, pH 5.5) was used as detection buffer to investigate the performance of electrodes. Phosphate buffered solution (PBS, pH 7.4) was prepared by using 0.1 M KH_2PO_4, 0.1 M Na_2HPO_4 and 0.1 M KCl. 5 mM

$[Fe(CN)_6]^{4-/3-}$ solution containing 0.1 M KCl was employed as a redox probe for cyclic voltammetry (CV) and electrochemical impedance spectroscopy (EIS) characterizations.

All of oligonucleotides and miRNAs were synthesized and purified by Sangon Biological Engineering Technology and Services Co., Ltd. (Shanghai, China). The sequences were listed in Table 1.

Table 1

2.2. Apparatus

Square wave voltammetry (SWV) and CV measurements were performed on a CHI 660D electrochemical workstation (Shanghai Chen Hua Instrument, Co., China). EIS measurements were conducted with a PARSTAT 4000 electrochemical workstation (Princeton Applied Research, USA). All electrochemical measurements were performed on a three-electrode system with modified glassy carbon electrode (GCE, Φ = 4mm) as working electrode, a saturated calomel as reference electrode and a platinum wire as auxiliary electrode. Scanning electron microscopy (SEM, Carl Zeiss Microscopy GmbH., Germany) and transmission electron microscopy (TEM, Tecnai G2 F20 S-Twin, USA) were used for characterizing the morphologies of various nanomaterials. P-ERCA assay was performed with a T100 TM Thermal Cycler (BioRad, USA).

2.3. Synthesis of $CoFe_2O_4$ MNPs

$CoFe_2O_4$ MNPs were prepared by solvothermal method [34]. Briefly, 0.032 g anhydrous $FeCl_3$ (5 mM) and 0.019 g $CoCl_2$ (2.5 mM) were dissolved in 8 mL

ethylene glycol, and kept stirring to form a clear orange solution. Subsequently, 0.144 g NaAc and 0.04 g PEG (M = 10000) were added into the above solution with vigorous stirring for 0.5 h. Later, it was sealed in autoclave with a tetrafluoroethylene liner and heated to 200 °C to react overnight. After reaction, it was cooled naturally to room temperature, and the black products ($CoFe_2O_4$ MNPs) were rinsed with ethanol and dried at 60 °C.

2.4. Preparation of the CP II bioconjugate (CP II/Au@$CoFe_2O_4$/Tb-Gra)

Preparation of Au@$CoFe_2O_4$: The obtained $CoFe_2O_4$ MNPs (1 mg) were firstly dissolved in ultrapure water (1 mL) containing PDDA (1%) and stirred for 4 h at ambient condition. After centrifugation at 8000 rpm for 20 min to remove surplus reagent, the product of PDDA modified $CoFe_2O_4$ MNPs was resuspended in 1 mL PBS. At the same time, gold nanoparticles (Au NPs, about 13 nm diameter) were prepared according to the previous protocol [35]. The PDDA modified $CoFe_2O_4$ MNPs solution was then added into 5 mL solution of the as-prepared Au NPs, and kept stirring for 5 h to obtain Au NPs decorated $CoFe_2O_4$ MNPs (abbreviated as Au@$CoFe_2O_4$ MNPs).

Graphene oxide (GO) was synthesized by Wang's method [36] and was further reduced (Gra) according to our previous work [37]. Then Tb (1 mg) was dispersed in 1 mg mL^{-1} of Gra solution (1 mL) with continuous stirring for 36 h to obtain Tb-Gra nanocomposites by a simple π-π stacking approach. After washing and centrifugating three times, the resulting Tb-Gra precipitate was resuspended in ultrapure water (1 mL) containing a proper amount of PEI and stirred for 2 h to obtain abundant -NH_2 groups

on the surface of Tb-Gra. Next, the as-prepared Au@$CoFe_2O_4$ was added into the above solution and the mixture was allowed to react for 4 h, obtaining the product of Au@$CoFe_2O_4$/Tb-Gra *via* strong amino-Au affinity. After magnetic separation, the synthesized product (Au@$CoFe_2O_4$/Tb-Gra) was slowly added into the probe immobilization buffer (IB) containing CP II (1 μM) to react overnight under softly stirring at 4 ℃. The obtained CP II bioconjugate (CP II/Au@$CoFe_2O_4$/Tb-Gra) was collected by employing an external magnetic field and finally dispersed in 1 mL of PBS.

2.5. P-ERCA reactions

1 μL of miR-21 with different concentrations (e.g. 0 fM, 1 fM, 10 fM, 100 fM, 1 pM, 10 pM, 100 pM, 1 nM and 2 nM) and 1 μL of padlock probe (1 nM) were mixed, then the mixture was denatured at 95 ℃ for 3 min and cooled slowly to room temperature. After annealing, 1 μL of T4 RNA ligase 2 (10 U), 2 μL of 10 × ligation buffer and 15 μL nuclease free water were added to the mixture to a 20 μL total reaction volume. The solution was further incubated at 37 ℃ for 2 h for ligation reactions. Finally, the amplification reaction was carried out at 30 ℃ for 6 h in a 40 μL reaction solution containing 20 μL of ligation reaction products, 1 μL of Phi29 DNA polymerase (10 U), 4 μL of 10 × polymerase reaction buffer, 0.4 μL of 100 × BSA, 1 μL of Nt.BbvCI (10 U), 4 μL of 10 × cut smart buffer, 2 μL of 10 mM dNTPs and 7.6 μL of nuclease free water. The finished products were stored at 4 ℃.

2.6. Fabrication of the electrochemical biosensor

To construct the electrochemical biosensor, the well-polished GCE was first

immersed in 2 mL of $HAuCl_4$ solution (1%) under the potential of -0.2 V for 30 s to gain a porous AuNPs layer. Next, the DpAu/GCE was submerged into CP I solution (1 μM, IB) and incubated overnight at room temperature to immobilize the CP I *via* Au-S affinity. After that, the CP I/DpAu/GCE was rinsed with ultrapure water and blocked with 1% HT solution. After every step, the modified electrode was extensively cleaned with ultrapure water slightly to remove the physical adsorption. Finally, the resulting biosensor was stored at 4 ℃ before use.

2.7. Experimental measurements

Electrochemical detection of miR-21: For target detection, the resulting electrode were incubated with the mixture of 10 μL of triggers at a certain concentration which is associated with the concentration of miR-21, and 10 μL of CP II bioconjugate was at 45 ℃ for 2 h. After rinsing with ultrapure water, the designed biosensor was detected in 0.1 M HAc-NaAc (pH 5.5) to evaluate SWV response.

SWV characterization was carried out in 0.1 M HAc-NaAc buffer (pH 5.5) with the potential ranged from 0.1 V to -0.45 V. The step of the modified electrode was characterized by CV and EIS. CV measurements were taken from -0.2 V to 0.6 V at a scan rate of 0.1 V s^{-1} in 0.1 M PBS (pH 7.4) containing 5 mM $[Fe(CN)_6]^{4-/3-}$ as redox probe. EIS measurements were carried out in 0.1 M PBS (pH 7.4) containing 5 mM $[Fe(CN)_6]^{4-/3-}$, with the alternative voltage of 5 mV and the frequency range of 0.01 Hz-100 KHz.

3. Results and discussion

3.1. Characterization of the different nanomaterials

196 The size and morphology of different nanomaterials are characterized by SEM
197 and TEM, as shown in Fig. 2. SEM image of the as-prepared $CoFe_2O_4$ MNPs exhibits
198 an irregular structure with piling up together (Fig.2A). Unexpectedly, after adding
199 PDDA into $CoFe_2O_4$ solution with stirring overnight at room temperature, SEM
200 (Fig.2B) and TEM (Fig.2C) images clearly reveal that the spherical particles are
201 formed with uniform sizes, porous structure and regular morphologies. TEM image of
202 Au@$CoFe_2O_4$/Tb-Gra nanocomposites in Fig.2D verifies that amount of Au NPs are
203 randomly attached onto the surface of $CoFe_2O_4$ sphere, and the formed Au@$CoFe_2O_4$
204 is wrapped with a layer of thin film of Tb-Gra, indicating the successful preparation of
205 Au@$CoFe_2O_4$/Tb-Gra. Fig.2E shows the photographic image of (D) in absence (a)
206 and presence (b) of external magnetic field. It can be observed that the prepared
207 Au@$CoFe_2O_4$/Tb-Gra can be easily dispersed into the aqueous solution and formed a
208 stable suspension (a). However, with the external magnetic field, the stable suspension
209 of (a) is aggregated together (b), demonstrating that the prepared
210 Au@$CoFe_2O_4$/Tb-Gra nanocomposites have a good magnetic response.

211 **Fig. 2**

212 ***3.2. Electrochemical behaviors of the biosensor***

213 To confirm the proposed biosensor fabrication process, electrochemical
214 characteristics of CV and EIS measurements are employed to investigate the interface
215 properties of surface-modified electrodes in 5 mM $[Fe(CN)_6]^{4-/3-}$ (acting as redox
216 probe), and the results are presented in Fig. 3A and Fig. 3B, respectively. The bare
217 GCE (Fig. 3A, curve a) exhibits a pair of well-defined redox peaks and the peak

current response is about 204 μA, corresponding to the typical redox property of $[Fe(CN)_6]^{4-/3-}$. After Au NPs are electrodeposited onto GCE, the current response dramatically increases to 276 μA (Fig. 3A, curve b), indicating that the excellent conductivity and large surface area of Au NPs could promote the electron transfer effectively. As expected, when CP I is successfully immobilized onto the surface of DpAu/GCE, a decreased current is detected (Fig. 3A, curve c). Followed by blocking with HT, a successive decline is observed (Fig. 3A, curve d). It is assumed that CP I and HT on the electrode would hinder the electron transfer tunnel. Finally, when the P-ERCA amplification product with the concentration of 100 pM miR-21 and CP II bioconjugate are introduced to the resulting electrode surface, the redox peak currents are even lower (Fig. 3A, curve e), thereby suggesting the successful construction of the biosensor. Fig. 3B illustrates EIS characterization of the different modified electrodes in 5 mM $[Fe(CN)_6]^{4-/3-}$ solution within the frequency range of 10^{-2} to 10^5 Hz. In EIS measurement, the semicircle diameter of EIS is equal to R_{et}. The bare GCE indicates a small semicircle (Fig. 3B, curve a), representing a low electron-transfer resistance. When Au NPs are electrodeposited on the GCE, the semicircle is nearly disappeared and the Nyquist diagram is approximately a straight line (Fig. 3B, curve b). Then, the successive assembling of CP I, blocking with HT, and the mixture of P-ERCA amplification product and CP II bioconjugate, the semicircle diameter increases gradually (Fig. 3B, curves c, d and e, respectively), which attributed to the retardance of the diffusion ferricyanide toward the electrode surface due to the formation of the insulating layer. Based on the observations above, EIS

characterization is in good accordance with those of CV.

Fig. 3

3.3. Optimization of experimental parameters

To achieve the optimal biosensing performance, experimental parameters including the concentration of CP I, hybridization reaction temperature and incubation time are investigated. Fig. 4A displays the SWV signal of the biosensor for immobilizing CP I with the concentration from 0.1 to 2 μM. We can see that the SWV response increases with increasing concentration of CP I, and the maximum current response occurs at 1 μM. Fig. 4B reveals the effect of hybridization reaction temperature on the performance of the biosensor from 36 to 48 °C. It can be noted that the current responses increase with the temperature rapidly up to 45 °C, and decrease slightly after above 45 °C. Therefore, 45 °C is adopted as the optimal reaction temperature for subsequent study. Finally, the influence of incubation time of the hybridization reaction is investigated by incubating the mixture of the P-ERCA products and CP II bioconjugate on the surface of HT/CP I/DpAu/GCE for 0.5, 1, 1.5, 2, 2.5 and 3 h, respectively. As shown in Fig. 4C, the current responses increase rapidly with the incubation time up to 2 h, and the trend flat out after exceeding 2 h. As a result, the optimal incubation time of hybridization reaction is determined to be 2 h.

Fig. 4

3.4. Performance of the electrochemical biosensor

3.4.1. Comparison of different signal amplification strategies

In order to evaluate the signal amplification ability of the proposed protocol, the resulting biosensors are used for the determination of miR-21 (100 pM) with different amplification strategies, and the results are depicted in Fig. 5. After HT/CP I/DpAu modified GCE incubation with CP II/Au/Tb-Gra without signal amplification, a relative low SWV signal is obtained (Fig. 5, curve a), corresponding to the reversible redox molecule of Tb. It is interesting to note that when CP II/Au/Tb-Gra is replaced by the proposed CP II bioconjugate (CP II/Au@$CoFe_2O_4$/Tb-Gra), a remarkable enhanced SWV signal is observed (Fig. 5, curve b). The result reveals the catalytic activity of $CoFe_2O_4$ MNPs towards Tb for signal amplification even in the absence of H_2O_2. The high-performance of $CoFe_2O_4$ MNPs to assist non-substrate nanoelectrocatalysis may attribute to simultaneously immobilize the catalyst ($CoFe_2O_4$ MNPs) and the redox molecule (Tb) on the electrode surface. Obviously, the interaction distance between $CoFe_2O_4$ MNPs and Tb is reduced, thus, the catalytic efficiency and sensitivity are significantly improved. On the other hand, to examine the signal amplification ability of P-ERCA assay, the resulting electrode was incubated with the mixture of P-ERCA amplification product and CP II/Au/Tb-Gra. Compared with the above mentioned curve a, an obvious amplified signal is noticed (Fig. 5, curve c), implying the excellent amplifying performance of P-ERCA procedure. The amplified signal may be ascribed to the multiple polymerization and nicking reactions, which produce plenty of new triggers to initiate multiple reaction cycles, thus giving a sensitive SWV response. More inspiringly, after the electrode was incubated with P-ERCA amplification product and the proposed CP II

bioconjugate, the maximum response appeared as can be seen in Fig. 5, curve d. The above results clearly demonstrate that the remarkable sensitivity of the proposed biosensor can be attributed to the $CoFe_2O_4$-assisted nanoelectrocatalysis and P-ERCA signal amplification.

Fig. 5

3.4.2. SWV responses and calibration curves

To assess the quantitative range and sensitivity of the miRNA biosensor, various concentrations of miR-21 were detected with the developed biosensor under the optimized experimental conditions (Fig. 6). It can be seen from Fig. 6A that the SWV response of the biosensor is enhanced gradually as the concentration of the miR-21 increases. In Fig. 6B, the calibration plot exhibits a good linear correlation with the logarithm values of target concentrations in the range of 1 fM to 2 nM. The linear regression equation is I (μA) = 0.936 lg$c$ (nM) + 8.804 with a detection limit of 0.3 fM (S/N = 3) and the correlation coefficient of r^2 = 0.998. The high sensitivity should be attributed to the high efficiency of P-ERCA and $CoFe_2O_4$ as nanoelectrocatalyst-assisted signal amplification, which increases the detection signal remarkably. In addition, the performance compared with the previous reports for miRNA detection was listed in Table 2, implying the satisfactory detection limit and linear range of the proposed biosensor.

Fig. 6

Table 2

3.4.3. Specificity and stability of the proposed biosensor

Specificity is of great importance to estimate the performance of the biosensor, especially for miRNAs as they have small size and sequence similarity with other miRNA in the RNA family. Herein, three different miRNAs (miR-141, tRNA and sRNA) as the interfering substances are employed, and the change of the SWV (ΔI) response is used to evaluate the selectivity and specificity of the as-proposed biosensor. Here, ΔI are given by $\Delta I = I - I_0$ (The background noise is recorded as I_0, while the SWV response is recorded as I toward different interferents). In Fig. 7A, no apparent change is obtained in comparison with that in the presence of miR-21. Although the high concentration of interfering substances (miR-141, tRNA and sRNA) are coexisted, the detection signal has also no remarkable difference. The above results indicate the high specificity and selectivity of the proposed assay for miR-21 detection.

Stability is another important factor to evaluate the performance of the biosensor. To examine whether the prepared biosensor could meet the needs of long testing process, the stability of the proposed biosensor was studied by using the same resultant electrode for intermittent SWV measurements at the same condition for 15 times. As shown in Fig. 7B, the SWV responses do not show any significant changes (*RSD* = 1.016%, *n* = 15). Furthermore, the long-term storage stability was also investigated by a batch of as-prepared electrodes (HT/CP I/DpAu/GCE), P-ERCA amplification product and CP II bioconjugate (CP II/Au@$CoFe_2O_4$/Tb-Gra) were stored at 4 ℃ and investigated over a period of 20 days. Every 2-5 day, the above electrodes were taken out to incubate with the mixture of 10 μL of P-ERCA

amplification product and 10 μL of CP II bioconjugate for 2 h, SWV responses of the resultant biosensors were recorded. As shown in Fig. 7C, it is found that no remarkable signal change is observed during the 5 days and the response retains 98.7% of its initial current. After storing for 20 days, it also maintains 90.3% of the original response. Thus, the above results clearly demonstrate that the stability of the proposed biosensor is favorable.

Fig. 7

3.4.4. Real sample analysis

To evaluate the analytical reliability and verify the potential application, the designed biosensor was studied by detecting miR-21 in total RNA (MCF-7, human breast cancer cell line). The total RNA was diluted to 100 ng μL^{-1}, and 1 μL sample was used for measurement. The amount of miR-21 in above RNA sample was estimated to be 2.97 amol (2.97 pM in 1 μL total RNA) according to the calibration curve (Fig. 6B). To further evaluate its performance in real sample analysis, different amounts of miR-21 (10, 30 and 50 pM, respectively) were spiked into total RNA for the assay. It can be seen that the recoveries are in the range of 103.1–110.9% (Table 3), which clearly demonstrates the potentiality of the proposed biosensor for miRNA detection in real samples.

Table 3

4. Conclusions

In summary, a high specificity and sensitivity electrochemical biosensor has been designed for miR-21 detection by employing P-ERCA assay and $CoFe_2O_4$ MNPs

electrocatalysis redox molecule for signal amplification. The redox probe of Au@$CoFe_2O_4$/Tb-Gra is easily prepared and acts as nanoelectrocatalyst for high-performance Tb catalysis, which not only reduces the interaction distance between catalyst ($CoFe_2O_4$ MNPs) and redox molecule (Tb), but also avoids the adding of any substrate in testing solution. The as-prepared probe shows good stability, sensitivity as well as accuracy for electrochemical detection of miR-21. More importantly, the present assays can be readily extended to other miRNAs or DNA detection by slightly changing the corresponding probe sequences, which holds great potential in bioanalysis research and early clinical diagnostics.

Acknowledgments

We gratefully acknowledge financial support from the NNSF of China (21473135 and 21605121), the Natural Science Foundation of Shanxi Province (15JS109 and 2016JQ2018), and the 59th China Postdoctoral Science Foundation Funded Project (2016M590966).

References

[1] C. Chen, D.A. Ridzon, A.J. Broomer, Z.H. Zhou, D.H. Lee, J.T. Nguyen, M. Barbisin, N.L. Xu, V.R. Mahuvakar, M.R. Andersen, K.Q. Lao, K.J. Livak, K.J. Guegler, Real-time quantification of microRNAs by stem-loop RT-PCR, Nucleic Acids Res. 33 (2005) e179.

[2] A. Lujambio, S.W. Lowe, The microcosmos of cancer, Nature 482 (2012) 347-355.

[3] R.X. Duan, X.L. Zuo, S.T. Wang, X.Y. Quan, D.L. Chen, Z.F. Chen, L. Jiang, C.H. Fan, F. Xia, Lab in a tube: ultrasensitive detection of microRNAs at the single-cell level and in breast cancer patients using quadratic isothermal amplification, J. Am. Chem. Soc. 135 (2013) 4604-4607.

[4] R.J. Deng, L.H. Tang, Q.Q. Tian, Y. Wang, L. Lin, J.H. Li, Toehold-initiated rolling circle amplification for visualizing individual microRNAs in situ in single cells, Angew. Chem. Int. Ed. 53 (2014) 2389-2393.

[5] Y.L. Wen, H. Pei, Y. Shen, J.J. Xi, M.H. Lin, N. Lu, X.Z. Shen, J. Li, C.H. Fan, DNA nanostructure-based interfacial engineering for PCR-free ultrasensitive electrochemical analysis of microRNA, Sci. Rep. 2 (2012)

[6] J.B. Li, S. Tan, R. Kooger, C.Y. Zhang, Y. Zhang, MicroRNAs as novel biological targets for detection and regulation, Chem. Soc. Rev. 43 (2014) 506-517.

[7] É. Várallyay, J. Burgyán, Z. Havelda, MicroRNA detection by northern blotting using locked nucleic acid probes, Nat. Protoc. 3 (2008) 190-196.

[8] H.H. Liu, X. Tian, Y.J. Li, C.A. Wu, C.C. Zheng, Microarray-based analysis of stress-regulated microRNAs in Arabidopsis thaliana, RNA 14 (2008) 836-843.

[9] J.Q. Yin, R.C. Zhao, K.V. Morris, Profiling microRNA expression with microarrays, Trends

Biotechnol. 26 (2008) 70-76.

[10] X.F. Jia, S.J. Dong, E.K. Wang, Engineering the bioelectrochemical interface using functional nanomaterials and microchip technique toward sensitive and portable electrochemical biosensors, Biosens. Bioelectron. 76 (2016) 80-90.

[11] J. Han, Y. Zhuo, Y.Q. Chai, Y. Xiang, R. Yuan, New type of redox nanoprobe: C_{60}-based nanomaterial and its application in electrochemical immunoassay for doping detection, Anal. Chem. 87 (2015) 1669-1675.

[12] Z.Y. Wang, Z.H. Dai, Carbon nanomaterial-based electrochemical biosensors: an overview, Nanoscale 7 (2015) 6420-6431.

[13] H.X. Ji, F. Yan, J.P. Lei, H.X. Ju, Ultrasensitive electrochemical detection of nucleic acids by template enhanced hybridization followed with rolling circle amplification, Anal. Chem. 84 (2012) 7166-7171.

[14] Y.T. Zhou, Q. Huang, J.M. Gao, J.X. Lu, X.Z. Shen, C.H. Fan, A dumbbell probe-mediated rolling circle amplification strategy for highly sensitive microRNA detection, Nucleic Acids Res. 38 (2010) e156.

[15] K. Hsieh, A.S. Patterson, B.S. Ferguson, K.W. Plaxco, H.T. Soh, Rapid, sensitive and quantitative detection of pathogenic DNA at the point of care through microfluidic electrochemical quantitative loop-mediated isothermal amplification, Angew. Chem. Int. Ed. 51 (2012) 4896-4900.

[16] Y.H. Hu, X.Q. Xu, Q.H. Liu, L. Wang, Z.Y. Lin, G.N. Chen, Ultrasensitive electrochemical biosensor for detection of DNA from bacillus subtilis by coupling target-Induced strand displacement and nicking endonuclease signal amplification, Anal. Chem. 86 (2014)

8785-8790.

[17] Q.Q. Tian, Y. Wang, R.J. Deng, L. Lin, Y. Liu, J.H. Li, Carbon nanotube enhanced label-free detection of microRNAs based on hairpin probe triggered solid-phase rolling-circle amplification, Nanoscale 7 (2015) 987-993.

[18] J.Y. Zhuang, W.Q. Lai, G.N. Chen, D.P. Tang, A rolling circle amplification-based DNA machine for miRNA screening coupling catalytic hairpin assembly with DNAzyme formation, Chem. Commun. 50 (2014) 2935-2938.

[19] M.M. Ali, F. Li, Z.Q. Zhang, K.X. Zhang, D.K. Kang, J.A. Ankrum, X.C. Le, W.A. Zhao, Rolling circle amplification: a versatile tool for chemical biology, materials science and medicine, Chem. Soc. Rev. 43 (2014) 3324-3341.

[20] H.Y. Liu, L. Li, L.L. Duan, X. Wang, Y.X. Xie, L.L. Tong, Q. Wang, B. Tang, High specific and ultrasensitive isothermal detection of microRNA by padlock probe-based exponential rolling circle amplification, Anal. Chem. 85 (2013) 7941-7947.

[21] X.J. Liao, Q.B. Wang, H.X. Ju, Simultaneous sensing of intracellular microRNAs with a multi-functionalized carbon nitride nanosheet probe, Chem. Commun. 50 (2014) 13604-13607.

[22] J.Y. Zhuang, D.Y. Tang, W.Q. Lai, M.D. Xu, D.P. Tang, Target-induced nano-enzyme reactor mediated hole-trapping for high-throughput immunoassay based on a split-type photoelectrochemical detection strategy, Anal. Chem. 87 (2015) 9473-9480.

[23] S. Chen, L.T. Chu, P.P. Yeung, Z.C. Zhao, Y.Y. Bao, M.S. Chan, P.K. Lo, T.H. Chen, Enzyme-free amplification by nano sticky balls for visual detection of ssDNA/RNA oligonucleotides, ACS Appl. Mater. Interfaces 7 (2015) 22821-22830.

[24] L. Artiglia, S. Agnoli, M.C. Paganini, M. Cattelan, G. Granozzi, TiO_2@CeO_x core-shell nanoparticles as artificial enzymes with peroxidase-like activity, ACS Appl. Mater. Interfaces 6 (2014) 20130-20136.

[25] M. Filice, O. Romero, J. Gutiérrez-Fernández, B. de las Rivas, J.A. Hermoso, J.M. Palomo, Synthesis of a heterogeneous artificial metallolipase with chimeric catalytic activity, Chem. Commun. 51 (2015) 9324-9327.

[26] Y.H. Lin, J.S. Ren, X.G. Qu, Catalytically active nanomaterials: a promising candidate for artificial enzymes, Acc. Chem. Res. 47 (2014) 1097-1105.

[27] Y. Leng, J.W. Zhao, P.P. Jiang, J. Wang, Amphiphilic polyoxometalate-paired polymer coated Fe_3O_4: magnetically recyclable catalyst for epoxidation of bio-derived olefins with H_2O_2, ACS Appl. Mater. Interfaces 6 (2014) 5947-5954.

[28] W.L. Gu, X. Deng, X.X. Gu, X.F. Jia, B.H. Lou, X.W. Zhang, J. Li, E.K. Wang, Stabilized, superparamagnetic functionalized graphene/Fe_3O_4@Au nanocomposites for a magnetically-controlled solid-state electrochemiluminescence biosensing application, Anal. Chem. 87 (2015) 1876-1881.

[29] Z.Z. Yang, Z. Zhang, Y.Z. Jiang, M.Q. Chi, G.D. Nie, X.F. Lu, C. Wang, Palladium nanoparticles modified electrospun $CoFe_2O_4$ nanotubes with enhanced peroxidase-like activity for colorimetric detection of hydrogen peroxide, RSC Adv. 6 (2016) 33636-33642.

[30] T.T. Zheng, Q.F. Zhang, S. Feng, J.J. Zhu, Q. Wang, H. Wang, Robust nonenzymatic hybrid nanoelectrocatalysts for signal amplification toward ultrasensitive electrochemical cytosensing, J. Am. Chem. Soc. 136 (2014) 2288-2291.

[31] V. Georgiadou, G. Makris, D. Papagiannopoulou, G. Vourlias, C. Dendrinou-Samara,

Octadecylamine-mediated versatile coating of $CoFe_2O_4$ NPs for the sustained release of anti-inflammatory drug naproxen and in vivo target selectivity, ACS Appl. Mater. Interfaces 8 (2016) 9345-9360.

[32] D. Gu, C.J. Jia, C. Weidenthaler, H.J. Bongard, B. Spliethoff, W. Schmidt, F. Schüth, Highly ordered mesoporous cobalt-containing oxides: structure, catalytic properties, and active sites in oxidation of carbon monoxide, J. Am. Chem. Soc. 137 (2015) 11407-11418.

[33] R. Hao, R.J. Xing, Z.C. Xu, Y.L. Hou, S. Gao, S.H. Sun, Synthesis, functionalization, and biomedical applications of multifunctional magnetic nanoparticles, Adv. Mater. 22 (2010) 2729-2742.

[34] M.P. Reddy, A.M.A. Mohamed, One-pot solvothermal synthesis and performance of mesoporous magnetic ferrite MFe_2O_4 nanospheres, Microporous Mesoporous Mater. 215 (2015) 37-45.

[35] A. Ambrosi, M.T. Castañeda, A.J. Killard, M.R. Smyth, S. Alegret, A. Merkoçi, Double-codified gold nanolabels for enhanced immunoanalysis., Anal. Chem. 79 (2007) 5232-5240.

[36] L. Wang, D. Wang, Z.H. Dong, F.X. Zhang, J. Jin, Interface chemistry engineering for stable cycling of reduced GO/SnO_2 nanocomposites for lithium ion battery, Nano Lett. 13 (2013) 1711-1716.

[37] J. Han, Y. Zhuo, Y.Q. Chai, Y.L. Yuan, R. Yuan, Novel electrochemical catalysis as signal amplified strategy for label-free detection of neuron-specific enolase, Biosens. Bioelectron. 31 (2012) 399-405.

[38] J.B. Li, P.H. Lei, S.J. Ding, Y. Zhang, J.R. Yang, Q. Cheng, Y.R. Yan, An enzyme-free surface plasmon resonance biosensor for real-time detecting microRNA based on allosteric

effect of mismatched catalytic hairpin assembly, Biosens. Bioelectron. 77 (2016) 435-441.

[39] Y.S. Guo, Y.J. Wang, G.X. Yang, J.J. Xu, H.Y. Chen, MicroRNA-mediated signal amplification coupled with GNP/dendrimers on a mass-sensitive biosensor and its applications in intracellular microRNA quantification, Biosens. Bioelectron. 85 (2016) 897-902.

[40] W. Ma, B. Situ, W.F. Lv, B. Li, X.M. Yin, P. Vadgama, L. Zheng, W. Wang, Electrochemical determination of microRNAs based on isothermal strand-displacement polymerase reaction coupled with multienzyme functionalized magnetic micro-carriers, Biosens. Bioelectron. 80 (2016) 344-351.

[41] Y.M. Wu, K. Sheng, Y.Q. Liu, Q. Yu , B.X. Ye, Enzyme spheres as novel tracing tags coupled with target-induced DNAzyme assembly for ultrasensitive electrochemical microRNA assay, Anal. Chim. Acta 948 (2016) 1-8.

[42] Y. Li, R. Tian, X.W. Zheng, R.F. Huang, Amplified electrochemical detection of nucleic acid hybridization via selective preconcentration of unmodified gold nanoparticles, Anal. Chim. Acta 934 (2016) 59-65.

[43] J. Li, J.J. Zhao, S.T. Li, L.L. Zhang, Y. Huang, S.L. Zhao, Y.M. Liu, Electrophoresis separation assisted G-quadruplex DNAzyme-based chemiluminescence signal amplification strategy on a microchip platform for highly sensitive detection of microRNA, Chem. Commun. 52 (2016) 12806-12809.

Figure captions:

Fig. 1. Schematic illustration of P-ERCA assay and $CoFe_2O_4$ MNPs-assisted non-substrate nanoelectrocatalysis for miR-21 detection. (A) Fabrication of CP II/Au@$CoFe_2O_4$/Tb-Gra probe (CP II bioconjugate) and (B) P-ERCA reaction.

Fig. 2. SEM images of (A) $CoFe_2O_4$ and (B) PDDA coating with $CoFe_2O_4$. TEM images of (C) PDDA coating with $CoFe_2O_4$ and (D) Au@$CoFe_2O_4$/Tb-Gra nanocomposites. (E) The photographic image of (D) in absence (a) and presence (b) of external magnetic field.

Fig. 3. The curves of CV (A) and EIS (B) are different modified electrodes performed in PBS (pH 7.4) containing 5 mM $[Fe(CN)_6]^{4-/3-}$ as redox probe: (a) bare GCE, (b) DpAu/GCE, (c) CP I/DpAu/GCE, (d) HT/CP I/DpAu/GCE, (e) after (d) incubated with the mixture of P-ERCA amplification product and CP II bioconjugate.

Fig.4. Influence of the concentration of CP I (A), hybridization reaction temperature (B) and incubation time (C) of the biosensor for the detection of 100 pM miR-21 in HAc-NaAc buffer solution (pH 5.5).

Fig. 5. SWV responses of the resulting electrodes for the detection of miR-21 (100 pM) with different signal amplification strategies. After HT/CP I/DpAu modified GCE (a) only incubation with CP II/Au/Tb-Gra without signal amplification; (b) incubation with CP II/Au@$CoFe_2O_4$/Tb-Gra ($CoFe_2O_4$ MNPs-assisted signal amplification strategy); (c) incubation with the mixture of P-ERCA amplification product and CP II/Au/Tb-Gra (P-ERCA-assisted signal amplification); (d) incubation with the mixture of P-ERCA amplification product and CP II/ Au@$CoFe_2O_4$/Tb-Gra ($CoFe_2O_4$ MNPs and P-ERCA-assisted signal amplification).

Fig. 6. (A) SWV curves of the resulting biosensor incubation with various P-ERCA reaction

products with different concentrations of miR-21 from (a) to (i): 0 fM, 1 fM, 10 fM, 100 fM, 1 pM, 10 pM, 100 pM, 1 nM, 2 nM, respectively, and then incubation with CP II/ Au@$CoFe_2O_4$/Tb-Gra. The SWV signals were measured in HAc-NaAc buffer solution (pH 5.5). (B) The corresponding calibration curve of the biosensor for miR-21 assay.

Fig. 7. (A) Selectivity investigation for miR-21 detection against the interference nucleic acids: miR-141 (1 nM), tRNA (1 nM), sRNA (1 nM), miR-21 (100 pM) and mixture (containing 1 nM miR-141, 1 nM tRNA, 1 nM sRNA, 100 pM miR-21), respectively. (B) Stability of the as-proposed biosensor incubated with 100 pM miR-21 for intermittent SWV scanning (n = 15). (C) The longterm storage stability of the as-prepared electrodes (HT/CP I/DpAu/GCE) incubated with the mixture of P-ERCA amplification product and CP II bioconjugate over a period of 20 days (error bars, SD; n = 3). All SWV signals were measured in HAc-NaAc buffer solution (pH 5.5).

Table 1. Sequences of the oligonucleotides used in this study.

Table 2. Comparison with various electrochemical methods for the detection of miRNA.

Table 3. The recoveries of the proposed method *via* spiking miRNA-21 into total RNA of MCF-7.

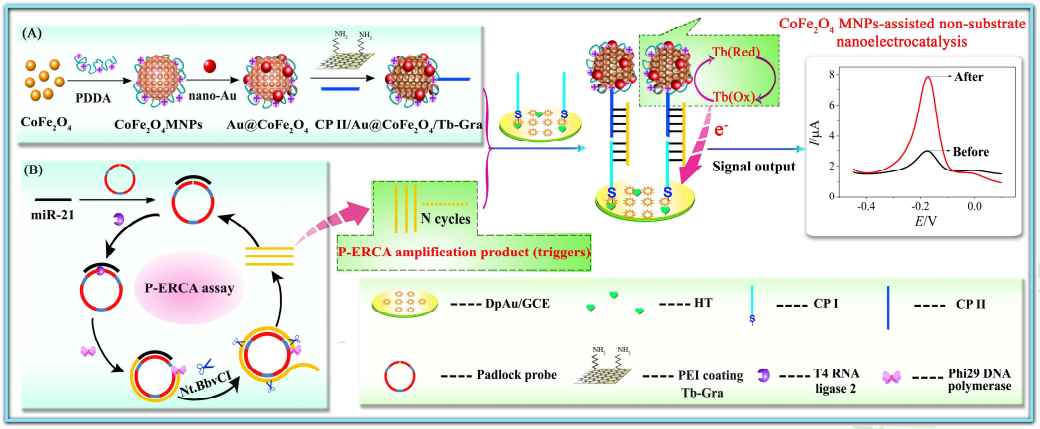

Fig. 1. Schematic illustration of P-ERCA assay and $CoFe_2O_4$ MNPs-assisted no substrate nanoelectrocatalysis for miR-21 detection. (A) Fabrication of CP II/Au@$CoFe_2O_4$/Tb-Gra probe (CP II bioconjugate) and (B) P-ERCA reaction.

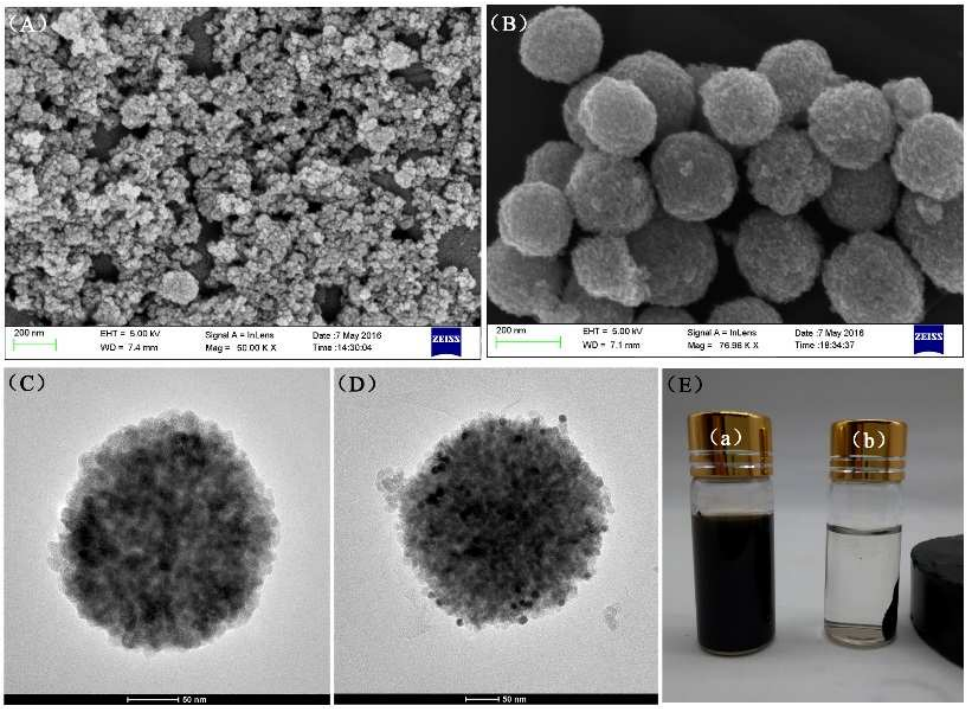

Fig. 2. SEM images of (A) $CoFe_2O_4$ MNPs and (B) PDDA coating with $CoFe_2O_4$ MNPs. TEM images of (C) PDDA coating with $CoFe_2O_4$ MNPs and (D) Au@$CoFe_2O_4$/Tb-Gra nanocomposites. (E) The photographic image of (D) in absence (a) and presence (b) of external magnetic field.

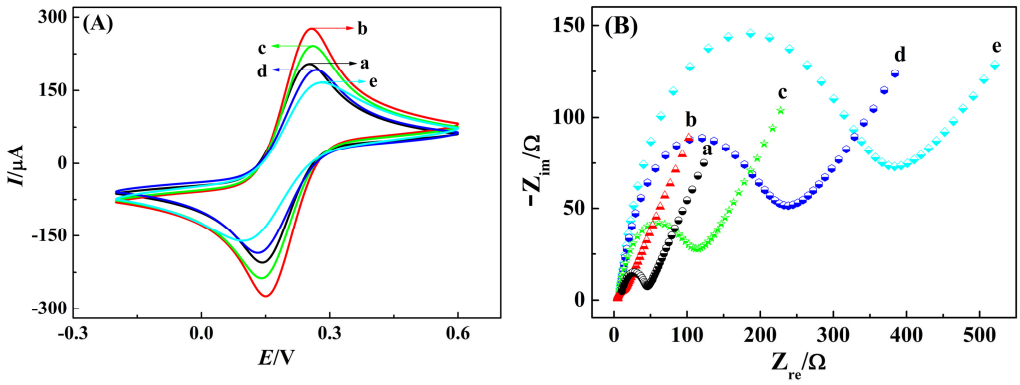

Fig. 3. The curves of CV (A) and EIS (B) are different modified electrodes performed in PBS (pH 7.4) containing 5 mM $[Fe(CN)_6]^{4-/3-}$ as redox probe: (a) bare GCE, (b) DpAu/GCE, (c) CP I/DpAu/GCE, (d) HT/CP I/DpAu/GCE, (e) after (d) incubated with the mixture of P-ERCA amplification product and CP II bioconjugate.

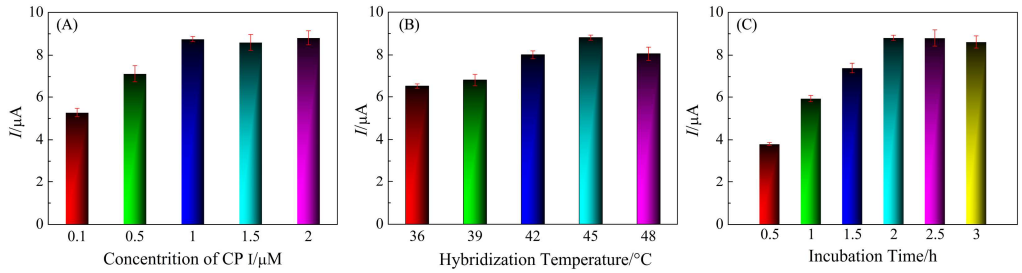

Fig.4. Influence of the concentration of CP I (A), hybridization reaction temperature (B) and incubation time (C) of the biosensor for the detection of 100 pM miR-21 in HAc-NaAc buffer solution (pH 5.5).

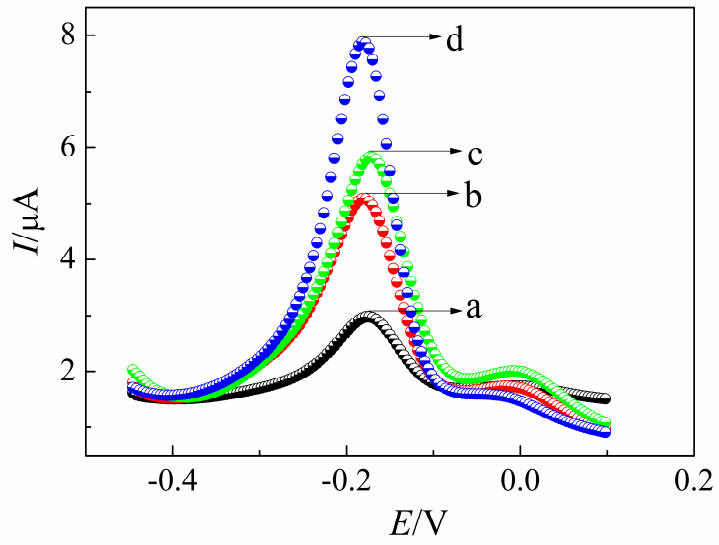

Fig. 5. SWV responses of the resulting electrodes for the detection of miR-21 (100 pM) with different signal amplification strategies. After HT/CP I/DpAu modified GCE (a) only incubation with CP II/Au/Tb-Gra without signal amplification; (b) incubation with CP II/Au@$CoFe_2O_4$/Tb-Gra ($CoFe_2O_4$ MNPs-assisted signal amplification strategy); (c) incubation with the mixture of P-ERCA amplification product and CP II/Au/Tb-Gra (P-ERCA-assisted signal amplification); (d) incubation with the mixture of P-ERCA amplification product and CP II/ Au@$CoFe_2O_4$/Tb-Gra ($CoFe_2O_4$ MNPs and P-ERCA-assisted signal amplification).

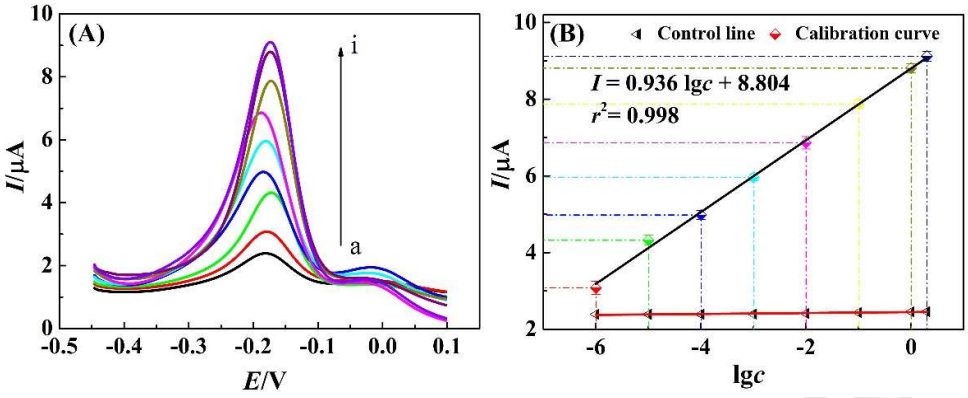

Fig. 6. (A) SWV curves of the resulting biosensor incubation with various P-ERCA reaction products with different concentrations of miR-21 from (a) to (i): 0 fM, 1 fM, 10 fM, 100 fM, 1 pM, 10 pM, 100 pM, 1 nM and 2 nM, respectively, and then incubation with CP II/Au@$CoFe_2O_4$/Tb-Gra. The SWV signals were measured in HAc-NaAc buffer solution (pH 5.5). (B) The corresponding calibration curve of the biosensor for miR-21 assay.

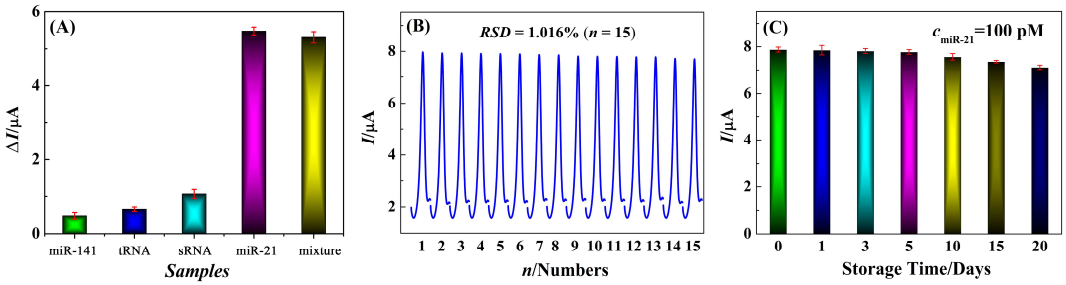

Fig. 7. (A) Selectivity investigation for miR-21 detection against the interference nucleic acids: miR-141 (1 nM), tRNA (1 nM), sRNA (1 nM), miR-21 (100 pM) and mixture (containing 1 nM miR-141, 1 nM tRNA, 1 nM sRNA, 100 pM miR-21), respectively. (B) Stability of the as-proposed biosensor incubated with 100 pM miR-21 for intermittent SWV scanning (n = 15). (C) The longterm storage stability of the as-prepared electrodes (HT/CP I/DpAu/GCE) incubated with the mixture of P-ERCA amplification product and CP II bioconjugate over a period of 20 days (error bars, SD; n = 3). All SWV signals were measured in HAc-NaAc buffer solution (pH 5.5).

668 **Table 1**. Sequences of the oligonucleotides used in this study.

Name	Sequences* (5'→ 3')
MiRNA-21 (miR-21)	UAG CUU AUC AGA CUG AUG UUG A
Padlock probe	Phosphate-CTGATAAGCTAGCTGAGGT CAACATCAGTCTGATAAGCTAGCTGA GGTCAACATCAGTCTGATAAGCTAGC TGAGGTCAACATCAGT
Capture probe I (CP I)	SH-$(CH_2)_6$-GGTCAACATCAGTC
Capture probe II (CP II)	TGATAAGCTAGCTGA-$(CH_2)_6$-NH_2
MiRNA-141 (miR-141)	UAA CAC UGU CUG GUA AAG AUG G
Single-base mismatched miRNA-21 (sRNA)	UAG CUU AUC AGA C<u>C</u>G AUG UUG A
Three-base mismatched miRNA-21 (tRNA)	UAG CU<u>A</u> AUC AGA C<u>C</u>G AUG U<u>A</u>G A

669 The underlined base(s) in the mismatched miR-21 is/are the different base(s) with miR-21;
670 the padlock probe is consist of a hybridization sequence to miR-21 (red) and a nicking site for
671 nicking endonuclease (blue).

672

673

674

675

676

677

678

679

680

681

682 **Table 2.** Comparison with various methods for the detection of miRNA.

Detection methods	Target	Linear range	Detection limit	Reference
surface plasmon resonance	miR-21	5 pM-100 nM	1 pM	[38]
time-dependent frequency	miR-203	10 pM-1 nM	1 pM	[39]
differential pulse voltammetry	miR-21	10 fM-10 nM	9 fM	[40]
differential pulse voltammetry	miR-24	3 fM-1 nM	0.2 fM	[41]
cyclic voltammetry	miR-let-7a	0.05-0.9 pM	16 fM	[42]
chemiluminescence	miR-30b	8 pM-20 nM	4.5 pM	[43]
square wave voltammetry	miR-21	1 fM-2 nM	0.3 fM	this work

683

684

685

686

687

688

689

690

691

692

693

694

695

696

697

698 **Table 3.** The recoveries of the proposed method *via* spiking miRNA-21 into total

699 RNA of MCF-7.

Sample	Spiking value/pM	Assayed value/pM	SD (*n*=3)	Recovery/%
total RNA (100 ng)	-	2.97	0.0488	-
1	10	14.06	0.2166	110.9
2	30	33.91	0.8139	103.1
3	50	56.39	1.0085	106.8

700

- $CoFe_2O_4$ MNPs-assisted non-substrate nanoelectrocatalysis was designed.
- A padlock probe-based exponential RCA assay for signal amplification was utilized.
- The as-prepared biosensor shows high specificity and sensitivity for miR-21.